Full three-dimensional direction-dependent X-ray scattering tomography

Zheyuan Zhu [a] and Shuo Pang*[a]
[a] College of Optics and Photonics (CREOL), University of Central Florida, 4304 Scorpius St, Orlando, FL, USA, 32816
*pang@creol.ucf.edu

ABSTRACT

Small-angle X-ray scattering (SAXS) detects the angular-dependent, coherently scattered X-ray photons, which provide improved contrast among different types of tissues or materials in medical diagnosis and material characterizations. By combining SAXS with computed tomography (CT), coherent scattering computed tomography (CSCT) enables the detection of spatially-resolved, material-specific scattering profile inside an extended object. However, conventional CSCT lacks the ability to distinguish direction-dependent coherent scattering signal, because of its assumptions that the materials are amorphous with isotropic scattering profiles. To overcome this issue, we propose a new CSCT imaging strategy, which can resolve the three-dimensional scattering profile for each object pixel, by incorporating detector movement into each CSCT projection measurement. The full reconstruction of the three-dimensional momentum transfer profile of a two-dimensional object has been successfully demonstrated. Our setup only requires a table-top X-ray source and a panel detector. The presented method demonstrates the potential to achieve low-cost, high-specificity X-ray tissue imaging and material characterization.

Keywords: Computed tomography, small-angle X-ray scattering, coherent scattering computed tomography

1. INTRODUCTION

Computed tomography (CT) is a widely used imaging technique in medical diagnosis. However, conventional CT cannot achieve high contrast among different types of soft tissues because it relies on the difference of X-ray attenuation coefficient, which varies little among soft tissues, to achieve contrast. By combining small-angle X-ray scattering with tomographic projection, coherent scattering computed tomography (CSCT), first introduced in 1987[1], is able to provide improved contrast among different materials inside a bulk object. A typical CSCT setup employs either angular-dispersive[2] or energy-dispersive[3] scheme, which all require collimators mounted in front of the detector at least in one direction to limit the scattering angle collected by each pixel, significantly limiting the collection efficiency. Moreover, conventional CSCT schemes assumes that the material is in the powder form, or amorphous, which possesses isotropic coherent scattering signal. Therefore, it can only reconstruct the coherent scattering profile in terms of the magnitude of momentum transfer rather than the momentum transfer vector. The magnitude of the momentum transfer is not adequate to fully characterize the scattering profile for some materials or biological tissues, such as bones[4], teeth[5] and brain tissues [6], which possess anisotropic scattering profile due to the partially ordered macrostructure in their compositions. Recent achievement in using synchrotron source to probe the three-dimensional real and momentum transfer space has been implemented[7], but the use of synchrotron radiation limits its application in the field of medical imaging. Here in our work, by incorporating detector movement into a pencil-beam angular dispersive CSCT, we demonstrate a simple, efficient and low-cost method to acquire full three-dimensional scattering information in an extended object.

2. THEORY

2.1 X-ray coherent scattering

The system setup and coordinates are shown in Fig.1. The direction of the incident X-ray beam is defined as $\hat{z}$. The origin of the laboratory coordinates is located at the rotation center O. The object and detector pixel coordinates, measured in terms of the laboratory coordinates, are denoted as $\mathbf{r} = (x, y, z)$ and $\mathbf{r}_d = (x_d, y_d, z_d)$, respectively. Due

to the small scattering angle, the mechanism of SAXS is dominated by coherent scattering. The number of coherent scattering photons coming from an object voxel located at $\mathbf{r}$ and collected by a detector pixel located $\mathbf{r}_d$ is given by [8]

$$dI = \frac{r_e^2}{2}\left(1+\cos^2\theta_{sc}\right) f(\mathbf{r},\mathbf{q})\mathrm{d}V\mathrm{d}\mathbf{q}\mathrm{d}\Omega, \tag{1}$$

where r_e is the classical electron radius. θ_{sc} is the scattering angle, and $\cos\theta_{sc}$ is approximately 1 for small scattering angle. $f(\mathbf{r},\mathbf{q}) = f_0(\mathbf{r},\mathbf{q})n(\mathbf{r})$, which is the product between the molecular form factor, $f_0(\mathbf{r},\mathbf{q})$, and the density of scatter, $n(\mathbf{r})$. $\mathrm{d}V = A\mathrm{d}z$, which represents the volume of the object voxel illuminated by the X-ray beam with cross-section area A. $\mathrm{d}\Omega = \Delta^2 / \left|\mathbf{r}_d - \mathbf{r}\right|^2$, which denotes the solid angle spanned by the detector pixel with size Δ. The momentum transfer, $\mathbf{q}$, represents the change between the incident and scattered wave vector. Given an object voxel located at $\mathbf{r}$, the momentum transfer of this voxel that causes the photon deviation onto the detector pixel located at $\mathbf{r}_d$ is

$$\mathbf{q} = \frac{E_0}{2hc}\left(\frac{\mathbf{r}-\mathbf{r}_d}{\left|\mathbf{r}-\mathbf{r}_d\right|} - \hat{z}\right), \tag{2}$$

where E_0 is the energy of incident X-ray, h and c are the Planck constant and speed of light, respectively. $\hat{z}$ denotes the unit vector along z direction, in which the incident X-ray beam is traveling.

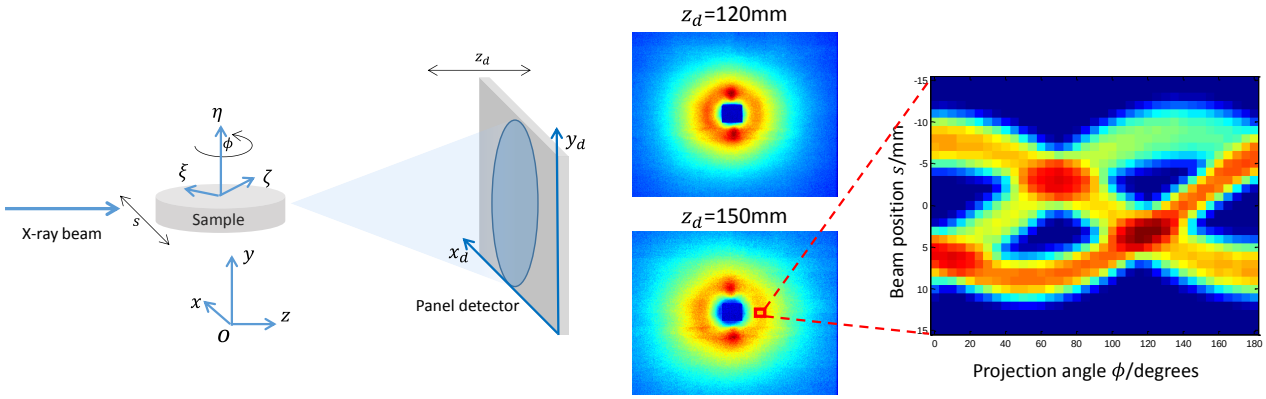

Figure 1: System setup and measurement. The X-ray is generated from a copper anode X-ray tube and collimated to a pencil beam. The object is mounted on rotation and translation stage that are used for CT projection scan across the pencil beam. A panel detector is mounted on a translation stage that moves along the direction of the beam. The resulting five-dimensional data consists of a three-dimensional array of detector pixels, each capturing a 2D sinogram from CT scan.

2.2 System model

To facilitate the discussion, a separate object coordinate system, (ξ,η,ζ), is established based on the geometric center of the object. It translates and rotates as the object is scanned across the pencil beam. Under projection angle $\phi = 0$, the object coordinates co-align with the laboratory coordinates. To completely determine a two-dimensional object with three-dimensional momentum transfer space expressed in the object coordinates, $f(\xi,\zeta,q_\xi,q_\eta,q_\zeta)$, the measurement covering 5 dimensions is required. Like conventional CT, object translation and rotation are utilized to resolve the 2 spatial dimensions of the object. To fully capture the 3D momentum transfer space of each hit pixel along the ray, an additional degree of translation of detector plane is added along z direction. These three degrees of freedom on the detector essentially covers the information from the entire 3D momentum transfer space of each scatter. Under projection angle ϕ and beam offset s, the total photon count g on the detector pixel at $\mathbf{r}_d = (x_d, y_d, z_d)$ is an integral in $(\mathbf{r},\mathbf{q})$ space along the parametric curve $\Gamma(t)$ defined in equation (2)

$$g(x_d, y_d, z_d, s, \phi) = \int_{\Gamma(t)} r_e^2 f(\mathbf{r}, \mathbf{q}) \delta\left[\mathbf{q} - \frac{E}{hc}\left(\frac{\mathbf{r_d} - \mathbf{r}}{|\mathbf{r_d} - \mathbf{r}|} - \hat{z}\right)\right] \frac{\Delta^2}{|\mathbf{r_d} - \mathbf{r}|^2} \mathrm{d}V\mathrm{d}\mathbf{q}, \tag{3}$$

where, in terms of the object coordinates, the following relation can be derived according to the measurement geometry under small-angle approximation

$$\begin{aligned} x &= s\cos\phi + (z_d - t)\sin\phi \\ y &= -s\sin\phi + (z_d - t)\cos\phi \\ q_\xi &= \frac{E}{2hc}\frac{x_d}{t}\sin\phi \\ q_\eta &= \frac{E}{2hc}\frac{y_d}{t} \\ q_\zeta &= \frac{E}{2hc}\frac{x_d}{t}\cos\phi \end{aligned}, \tag{4}$$

where s is the offset between beam path and rotation center; t denotes the distance from the object pixel to the detector plane, and z_d is the distance between detector plane and the rotation center. Equation (3) defines a linear mapping between $(\xi, \zeta, q_\xi, q_\eta, q_\zeta)$ and (x_d, y_d, z_d, s, ϕ), which can be expressed in a matrix form $\mathbf{g} = \mathbf{Hf}$ after discretizing the object and measurement into vectors.

3. EXPERIMENTS

In order to build our directional-dependent CSCT setup illustrated in Fig.1, we employed a copper-anode X-ray tube (XRT60, Proto Manufacturing) as the narrow band X-ray source, which emits a quasi-monochromatic spectrum centering around 8keV. Two 2mm pinholes placed downstream the source collimate the X-ray into a pencil beam. The sample is mounted on a rotational stage (RV1200P, Newport) and a translation stage (UTM150CC, Newport) for a pencil-beam CT scan. The step size of the translation stage was set to 1mm to match the Nyquist interval given the 2mm size of our X-ray beam. The scattered X-rays emerging from the sample was captured by a panel detector (1215CF-MP, Rayence), which is also mounted on a translation stage (UTM150CC, Newport) to scan a series of 2D scattering patterns under different distances, z_d, to the sample. The detector consists of 2352 by 2944 pixels in the horizontal and vertical direction respectively, with each pixel being $50\mu\mathrm{m} \times 50\mu\mathrm{m}$ in size. The position of the detector was carefully aligned in a way that the pencil beam would always hit its center as it moves along the direction of beam. The central $10\mathrm{mm} \times 10\mathrm{mm}$ region on the detector was covered by a beam stop made of 1/8inch-thick lead sheet pasted on an aluminum plate. The sample consists of three isolated cylindrical bulks made of butter, Teflon wrap and water, each being approximately 7mm in diameter and separated 10mm apart from each other. The Teflon wrap was tilted in the (ξ, η) plane for 5 degrees against the vertical direction. The sample was translated across the pencil beam for 30mm at a step size of 1mm, and rotated every 5 degrees to cover the projection angles from 0 to 180 degrees. The distance between the detector and the sample was changed from 120mm to 150mm at a step size of 3mm to capture a series of 2D scattering profiles along z direction. These movements generate a 3D array of detector pixels, each embedded with a sinogram as the sample undergoes normal CT scan.

4. RESULTS AND CONCLUSION

A CT image, shown in Fig. 3(a), demonstrates the general morphology of the sample used for this experiment. The full 3D momentum transfer space within this object is reconstructed by inverting the linear forward model described in Sec.2.2 using maximum-likelihood estimation. Fig. 3(b)-(d) show the reconstructed spatial profile corresponding to three different 3D momentum transfer vectors, under which an improved contrast among different types of materials can be observed. Under low momentum transfers, butter is the dominant scatter while Teflon only exhibit strong scattering along the q_η direction. As the momentum transfer increases, both butter and Teflon become weaker, while water gains

more coherent scattering intensity, eventually inverting its contrast with butter. Fig. 3(e),(f) cuts through the (q_ξ, q_η) plane in the three-dimensional momentum transfer space for butter and water, which all exhibit isotropic scattering profile. Fig. 3(g),(h) show the strong anisotropic scattering profile of the Teflon wrap in (q_ξ, q_η) plane, measured under 0 degree projection, and (q_ζ, q_η) plane, measured under 90 degree projection. The orientation of two scattering peaks from Teflon indicates the tilt angle under different projections. Since the Teflon wrap was not tilted in the (ζ, η) plane, two peaks align vertically under 90 degree projection; while for 0 degree projection, the tile in the (ξ, η) plane can be clearly observed.

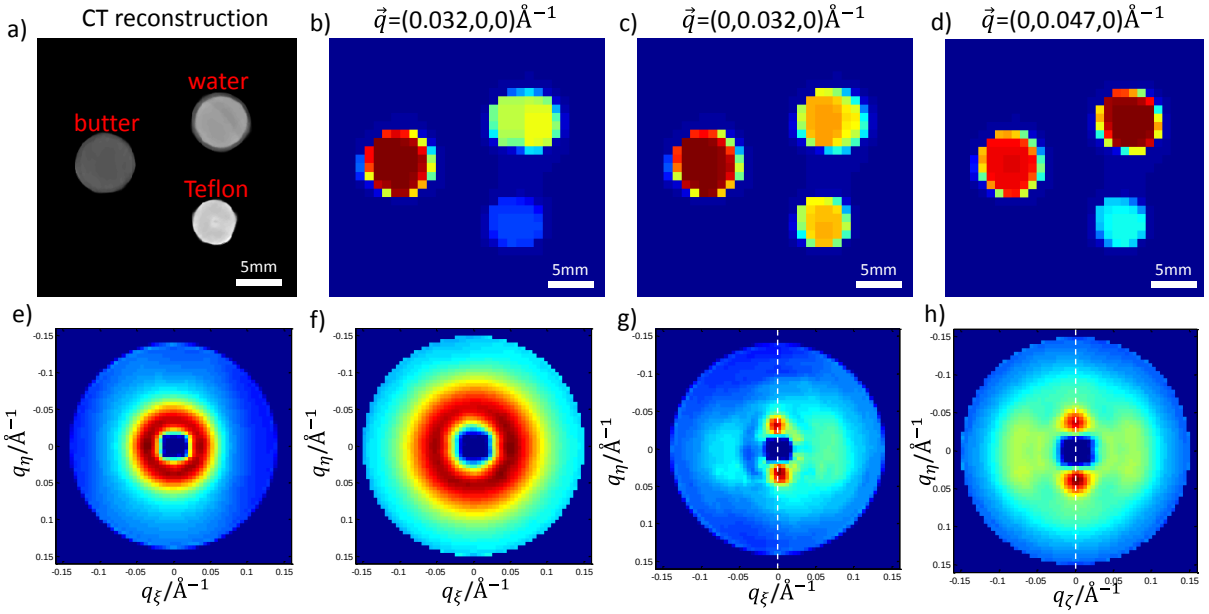

Figure 2: Reconstruction of the full three-dimensional momentum transfer space of a 2D object. (a) CT image of the sample. (b)-(d) Spatial profile of the object showing different contrast under vector momentum transfers , respectively. (e), (f) coherent scattering profile in (q_ξ, q_η) plane from a single pixel of butter and water inside the object. (g), (h) Scattering profile of Teflon in (ξ, η) and (ζ, η) plane, respectively.

5. CONCLUSION

In conclusion, we have developed a method to implement table-top direction-dependent X-ray scattering tomography that can obtain full 3D scattering information of each pixel in a 2D object. Compared with conventional CSCT methods, our system is able to capture the angular-dependent coherent scattering textures with high collection efficiency using only a low-brilliance table-top X-ray source. We expect our method developed here to become a low-cost, material-specific imaging modality with potential applications in the field of medical diagnosis and material characterization.

REFERENCES

[1] Harding, G., Kosanetzky, J.., Neitzel, U., "X-Ray-Diffraction Computed-Tomography," Med. Phys. **14**(4), 515–525 (1987).

[2] Cui, C. W., Jorgensen, S. M., Eaker, D. R.., Ritman, E. L., "Direct three-dimensional coherently scattered x-ray microtomography," Med. Phys. **37**(12), 6317–6322 (2010).

[3] Kosanetzky, G. H. and M. N. and J., "Energy-dispersive X-ray diffraction tomography," Phys. Med. Biol. **35**(1), 33 (1990).

[4] Fratzl, P., Jakob, H. F., Rinnerthaler, S., Roschger, P.., Klaushofer, K., "Position-Resolved Small-Angle X-ray Scattering of Complex Biological Materials," J. Appl. Crystallogr. **30**(5 Part 2), 765–769 (1997).

[5] Egan, C. K., Jacques, S. D. M., Di Michiel, M., Cai, B., Zandbergen, M. W., Lee, P. D., Beale, A. M.., Cernik, R. J., "Non-invasive imaging of the crystalline structure within a human tooth.," Acta Biomater. **9**(9), 8337–8345 (2013).

[6] Finet, M. D. F. and R. F. and C. F. and A. T. and M. G. and S., "Structural characterization of the human cerebral myelin sheath by small angle x-ray scattering," Phys. Med. Biol. **53**(20), 5675 (2008).

[7] Schaff, F., Bech, M., Zaslansky, P., Jud, C., Liebi, M., Guizar-Sicairos, M.., Pfeiffer, F., "Six-dimensional real and reciprocal space small-angle X-ray scattering tomography," Nature **527**(7578), 353–356, Nature Publishing Group, a division of Macmillan Publishers Limited. All Rights Reserved. (2015).

[8] Pang, S., Zhu, Z., Wang, G.., Cong, W., "Small-angle scatter tomography with a photon-counting detector array," Phys. Med. Biol. **61**(10), 3734 (2016).